RSC Advances

PAPER

View Article Online
View Journal | View Issue

Cite this: *RSC Adv.*, 2022, **12**, 33215

Preparation of stimuli responsive microgel with silver nanoparticles for biosensing and catalytic reduction of water pollutants

Sara Zahid,[a] A. Khuzaim Alzahrani,*[b] Nadeem Kizilbash,[b] Jaweria Ambreen,[c] Muhammad Ajmal,*[d] Zahoor H. Farooqi[e] and Muhammad Siddiq[a]

Received 31st August 2022
Accepted 15th November 2022

DOI: 10.1039/d2ra05475b

rsc.li/rsc-advances

Herein, we report poly(*N*-isopropylacrylamide/2-acrylamido-2-methylpropane sulfonic acid) microgel fabricated with silver nanoparticles. The identification of copolymerization and functional groups in the bare microgel and those fabricated with silver nanoparticles was examined by Fourier transform infrared spectroscopy. The pH and temperature sensitivity of microgels was studied using dynamic light scattering. Thermogravimetric analysis was carried out to study the thermal stability. X-Ray diffraction patterns indicated the amorphous nature of bare microgel and crystalline nature of those containing silver nanoparticles. A bathochromic shift was found in the surface plasmon resonance of silver nanoparticles present in microgel with increase in pH of the medium. Moreover, the microgel containing silver nanoparticles served as an effective catalyst for reducing the toxic nitroaromatic pollutants and carcinogenic dyes. The microgel containing silver nanoparticles also showed good capability to serve as biosensor for the detection of hydrogen peroxide.

1. Introduction

Water treatment and purification has become an important concern globally. Among the various water pollutants, nitro-aromatic compounds and azo dyes have been found to cause many diseases in the living organisms and their removal from water has become necessary and big challenge to the ease of method and economic viewpoint.[1–3] Multiple strategies have been devised by researchers in the past few years. Among them, polymer microgels have been found important scaffolds for this purpose.[4] Polymer microgels are three dimensional polymeric networks containing water as a dispersed phase. They can extract many water pollutants such as toxic metal ions and dyes by sorption.[5,6] Microgels can be designed with metal ion binding functional groups which enable them to extract high amounts of metal ions for the purity of aqueous medium.[7] The metal ions loaded in the microgels can be further converted into the nanoparticles by *in situ* reduction in the microgel networks.[8] The microgels containing suitable metal nanoparticles can be further employed as catalyst for the fast reduction of many water contaminants which cannot be removed from water by sorption.[9,10] The metal nanoparticles show excellent catalytic,[11] electrical,[12] optical,[13] and anti-bacterial properties[14] but they are not stable themselves. To achieve the stability, these metal nanoparticles can be fabricated within the microgel networks. The functional groups of microgel network and the fabricated metal nanoparticles are involved in the mutual electronic interactions which result in the stabilization of metal nanoparticle within the microgel networks.[15] These microgels fabricated with suitable metal nanoparticles can be used as catalysts for the degradation/reduction of many water pollutants. Among the various metal nanoparticles, AgNPs have been focused by many scientists owing to their low and multiple properties including antibacterial,[16] catalytic,[17,18] optical sensing,[19] chemical sensing,[20] *etc.* The catalytic and optical properties of AgNPs can be tuned if they are embedded in the microgel network. When a microgel containing AgNPs is used as catalyst, the reaction takes place within the microgel network, and it depends on the rate of diffusion of reactants towards the microgel network. By changing the porosity of the microgel, the rate of diffusion of reactants towards the microgel and hence the rate of the catalytic reaction can be tuned.[21] Similarly, if temperature and pH of the sensitive microgel system is changed the SPR band of the AgNPs fabricated in that microgel system can be shifted which makes the system a sensor for pH and temperature.[22] If the AgNPs fabricated in a suitable microgel and the system is used as catalyst then recovery of this catalyst from a catalytic reaction medium can be done easily by simple filtration or quick centrifugation process.[23] Timo *et al.*[24] fabricated AgNPs in a microgel system and found it as

[a]*Department of Chemistry, Quaid-i-Azam University, Islamabad 45320, Pakistan*
[b]*Department of Medical Laboratory Technology, Faculty of Applied Medical Sciences, Northern Border University, Arar-91431, Saudi Arabia. E-mail: akaalz@nbu.edu.sa*
[c]*Department of Chemistry, COMSATS University Islamabad, Park Road, 45550, Islamabad, Pakistan*
[d]*Department of Chemistry, Division of Science and Technology, University of Education, Lahore, Pakistan. E-mail: m.ajmal65@yahoo.com*
[e]*School of Chemistry, University of the Punjab, Lahore 54590, Pakistan*

temperature sensitive catalyst for the reduction of 4-NP. Lazaros *et al.*[25] also reported the synthesis of AgNPs in a microgel system and their application as an efficient catalyst in the reduction of 4-NP. Similarly, Li *et al.*[26] prepared AgNPs in a microgel system to tune their optical properties and usefully designed a light controllable catalytically active system. In addition to their catalytic role, AgNPs have also been found to act as promising biosensor for the detection of H_2O_2, known as a versatile biomarker.[27] Recent investigations have shown that H_2O_2 is plays several important roles in biochemical procedures such as cell signaling.[27] For the effective disease diagnosis, and disease monitoring H_2O_2 is used as a reactive biomarker. In food industry, H_2O_2 is applied for the preservation of milk but its high concentration can damage the quality of milk by degradation of folic acid present in milk.[28] The higher concentration of H_2O_2 in food items may cause some life-threatening diseases such as cardiovascular disorder, diabetes, and cancer.[29] Therefore, development of reliable simple, and economical method for the detection of H_2O_2 is has become need of the hour. It has been reported that H_2O_2 can be detected with AgNPs in terms of change in intensity of absorbance at the maximum absorption wavelength of AgNPs.[18,30] So, AgNPs have potential for the colorimetric detection of H_2O_2. However, stability of AgNPs without affecting its sensing ability has been a great challenge. Thanks to the microgels for having potential to stabilize AgNPs without affecting their sensing and catalytic potential. Among the microgels used for the fabrication of AgNPs, NIPAM and acrylic/methacrylic acid based microgels have been used and various parameters have been reported to tune the stability, catalytic and optical activity of AgNPs. NIPAM can also be copolymerized with other monomers, but less attention has been given therefore the effect of other monomers on the fabrication and further applications AgNPs needs to be explored. In this context, we have prepared a microgel by copolymerizing NIPAM with AMPS and used to fabricate as well as stabilize the AgNPs within the microgel's network. Catalytic activity of this AgNPs–MG system has been explored in the reduction of azo dyes and nitroaromatic compounds. In addition, the AgNPs–MG system has also shown hydrogen peroxide sensing ability.

2. Materials and methods

2.1 Chemicals

N-Isopropylacrylamide (NIPAM, 97% Sigma-Aldrich) and 2-acrylamido-2-methylpropane sulfonic acid (AMPS, 99% Sigma-Aldrich) were used as monomers, *N*,*N*′-methylene-bis-acrylamide (MBA, 99% Sigma-Aldrich) was used as a cross-linker. Ammonium per sulfate (APS, 98% Sigma-Aldrich) was used as an initiator and sodium dodecyl sulfate (SDS, ≥98.5% BDH Chemicals) was used as a surfactant. Silver nitrate ($AgNO_3$, 99% Sigma-Aldrich) was used as a metal precursor. Sodium borohydride ($NaBH_4$, 98% Sigma-Aldrich) was employed as a reducing agent. 4-Nitrophenol (4-NP, 99% Sigma-Aldrich), 2-nitrophenol (2-NP, 98% Sigma-Aldrich), 2-nitroaniline (2-NA, 98% Sigma-Aldrich), methyl orange (MO, 85% Alpha Aesar), Methylene Blue (MB 82% Alpha Aesar), Eosin Y (EY, 82% Alpha Aesar) were used for catalytic degradation. Deionized water was prepared in the laboratory and used throughout this work.

2.2 Synthesis of bare p(NIPAM/AMPS) microgel

Free radical copolymerization was carried out to synthesize p(NIPAM/AMPS) microgel. The reaction mixture was prepared by adding 0.07 g SDS, 95 mL deionized water, 1.29 g NIPAM, 0.124 g AMPS and 0.037 g MBA in a three necked round bottom flask followed by its equipment with nitrogen inlet, condenser, and oil bath in the experimental assembly. The temperature of the reaction mixture was raised to 70 °C *via* an oil bath along with continuous stirring and nitrogen purging. After 30 minutes, 5 mL of 0.06 M APS solution was added in the reaction mixture and milky appearance was observed within five minutes. The reaction was further continued for 5 hours at 70 °C under constant stirring and nitrogen purging and then cooled down to room temperature. The product was transferred to dialysis membrane and dialysis was carried out for one week to remove the unreacted species. A cellulose membrane having molecular weight cutoff of 14 000 was used as dialysis membrane. The prepared bare p(NIPAM/AMPS) (BMG) microgel was dried at 100 °C for characterization.

2.3 *In situ* synthesis of silver nanoparticles in p(NIPAM/AMPS) microgel

Silver nanoparticles were prepared within the prepared BMG by *in situ* reduction of silver ions at room temperature. For this purpose, 10 mL of the as-prepared BMG was diluted with 20 mL deionized water and the reaction was carried out in the nitrogen atmosphere in a round bottom flask. After 30 minutes, 0.1 molar aqueous solution of silver nitrate was prepared and its 0.5 mL was added in the already diluted MBG and stirred for 1 hour along with nitrogen purging. In this AMPS to silver ions mol ratio was maintained as 1 : 6 to ensure the maximum loading of silver ions in BMG. Then, 0.05 g $NaBH_4$ dissolved in 5 mL distilled water was added and color of the reaction mixture turned yellow from colorless. The reaction was further stirred for 1 hour and then the BMG fabricated with AgNPs (AgNPs–MG) was dialyzed against deionized water for four hours.

2.4 Characterization techniques

Fourier transform infrared (FTIR) spectra were recorded with FTIR spectrophotometer Model RZX (PerkinElmer) to identify the functional groups in the BMG and AgNPs–MG. X-Ray diffractometer Model 3040/60 X'Pert PRO (PANalytical) was used to check the texture of the prepared BMG and AgNPs–MG. Dynamic laser light spectrometer (B1-200SM, Brookhaven Instrument) was used to find out hydrodynamic diameters. Thermogravimetric analyzer (TGA) (Mettler Tolledo 851e) was employed to find out thermal stability. The optical, catalytic, and sensing applications were studied with UV-visible spectrophotometer (Shimadzu 1700).

2.5 Catalytic reduction and chemical sensing study

The prepared AgNPs–MG was analyzed as catalyst in the reduction of 2-NP, 2-NP, 4-NP, MO, EY, and MB with $NaBH_4$ in

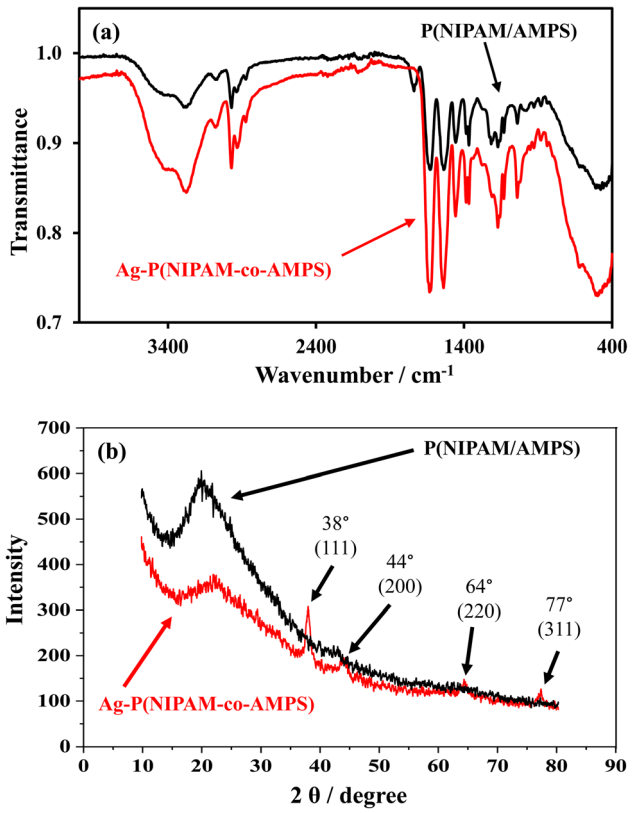

Fig. 1 (a) FTIR spectra and (b) XRD patterns of p(NIPAM/AMPS) and Ag–p(NIPAM/AMPS).

aqueous medium. UV-visible spectrophotometer was utilized to observe the progress of these catalytic reactions. The catalytic reduction was conducted with 40 ml aqueous solution of either of 0.001 M 4-NP, 0.001 M 2-NP, 1 mM 2-NA, 4×10^{-4} M MO, 4×10^{-4} M EY and 1.6×10^{-4} M MB. The solution was added with a calculated amount of $NaBH_4$ so that its concentration with respect to $NaBH_4$ was hundred times larger as compared to that of nitrocompound or dye. A certain amount of AgNPs–MG (100 μL for nitrocompound and 400 μL for dye) was included as catalyst. The reaction was accomplished at constant temperature by placing the reaction container in a thermostat. During the catalytic reaction, 0.5 ml of the sample was taken out from the reaction mixture after certain time intervals followed by dilution with deionized water (15 times dilution for each of 4-NP, MO, EY and MB, 8 times dilution for each of 2-NP and 2-NA) and subjected to record UV-Vis spectrum. Effect of amount of catalyst was studied by conducting the reduction of 4-NP using different amount of catalyst *i.e.*, 100 μL, 200 μL, 300 μL and 400 μL. Effect of temperature was also examined in the reduction of 4-NP by keeping catalyst amount constant and varying the temperatures (293, 303, 313, 323, and 333 K).

For hydrogen peroxide sensing, 0.5 mL of the aqueous solution of H_2O_2 (100, 500, 1000, 1500, 2000, 2500 and 3000 μM) was added to 3.5 mL of AgNPs–MG. UV-visible spectra were recorded for each concentration till 30 minutes.

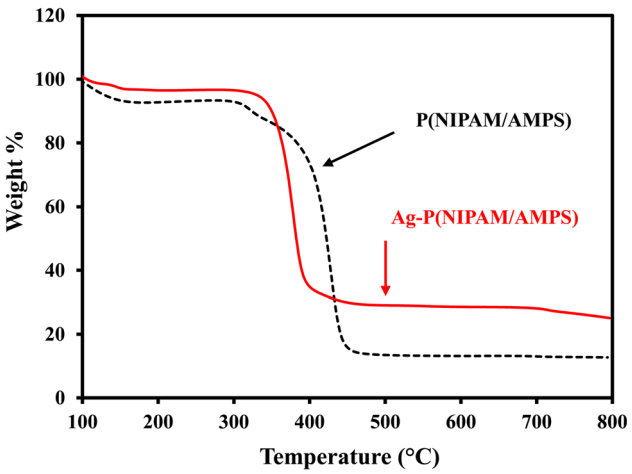

Fig. 2 Thermograms of p(NIPAM/AMPS) and Ag–p(NIPAM/AMPS).

3. Results and discussion

3.1 Characterization of BMG and AgNPs–MG

To identify various functional groups, FTIR spectroscopy was used as a characterization technique. Fig. 1(a) illustrates the FTIR spectra of BMG and AgNPs–MG. A broad peak at 3292.06 cm^{-1} is because of the overlapping of stretching peaks from N–H in NIPAM and from O–H in AMPS. The C–H

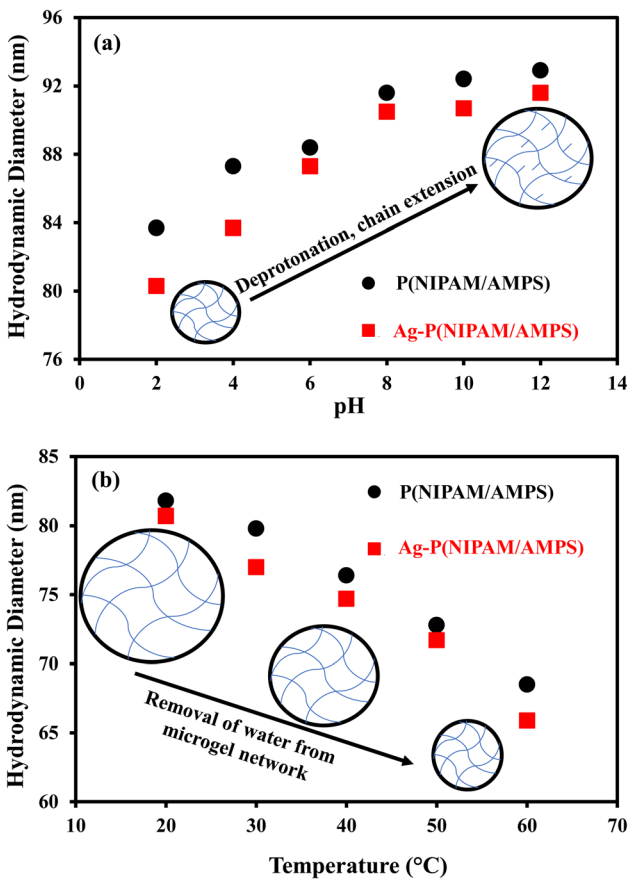

Fig. 3 (a) pH and (b) temperature responsive behavior of p(NIPAM/AMPS) and Ag–p(NIPAM/AMPS) along with the schematic illustration of the mechanism.

stretching peak was observed at 2927.76 cm^{-1} and the peak at 1633.06 cm^{-1} was ascribed to amide stretching. The peak at 1366.45 cm^{-1} corresponds to $CH(CH_3)_2$ stretching, the peak at 1016.87 cm^{-1} was assigned to stretching of $-SO_3$ in AMPS units. The typical peak of C=C at 1620 cm^{-1} was absent, which indicated that BMG was synthesized successfully. For AgNPs–MG some of the peaks were disappeared or changed slightly due to electronic interactions between electrons of polymeric functional groups and electrons of AgNP's such as the interactions present between amide and sulfonic acid groups of microgel and AgNPs. The electronic coordination interactions between lone pairs of functional groups (such as acrylamide and carbonyl) of microgel and the surface of metal nanoparticles have been investigated *via* X-ray photoelectron spectroscopy (XPS).[31] An electron donor–acceptor interaction between AgNPs and functional groups of microgel may also exist which can be identified by an increase in the binding energy when Ag atoms act as electron donor and a decrease in binding energy when Ag atoms act as electron accepter.[15] The stabilization of AgNPs in poly(*N*-isopropylacrylamide-*co*-acrylic acid) microgel *via* charge transfer from carbonyl groups to AgNPs have also been proved *via* XPS analysis by Dong *et al.*[15] The band from 3292.06 cm^{-1} is shifted to 3277.59 cm^{-1} due to formation of OH···AgNPs bonds. This OH···AgNPs bond can be developed by interaction of lone pairs of oxygen of hydroxyl group of water and Ag atoms present at the surface of AgNPs. Similar observations were reported by Han *et al.* and Bibi *et al.*[32,33]

It is a well-known fact that polymer hydrogels exhibit porous nature while AgNPs exhibit crystalline nature and a composite prepared by fabricating AgNPs in a polymer hydrogel network possess both the amorphous and crystalline properties.[23] The XRD patterns of BMG and AgNPs–MG are shown in Fig. 1(b). BMG exhibited a broad peak in the range of 14–26° 2θ values indicating its amorphous nature.[18,34] On the other hand, AgNPs–MG showed crystalline nature due to the AgNPs embedded within the microgel network. The diffraction peaks obtained at 38°, 44°, 64° and 77° correspond to miller indices (111), (200), (220) and (311) respectively which are characteristic for AgNPs with the face-centered cubic geometry.[18]

TGA analysis was done to investigate the thermal properties of the BMG and AgNPs–MG. TGA profiles of BMG and AgNPs–MG in the temperature range of 0 to 800 °C are shown in Fig. 2. A stepwise thermal degradation from 50 to 400 °C was observed for BMG. A slight weight loss of 8% was observed till 150 °C which can be associated to the removal of water molecules entrapped in BMG. A further weight loss in the temperature range of 340 to 380 °C was observed which can be ascribed to the thermal collapse of polymeric network. The TGA profile of AgNPs–MG showed that thermal degradation was initiated above 200 °C and overall, 15% less weight as compared to BMG

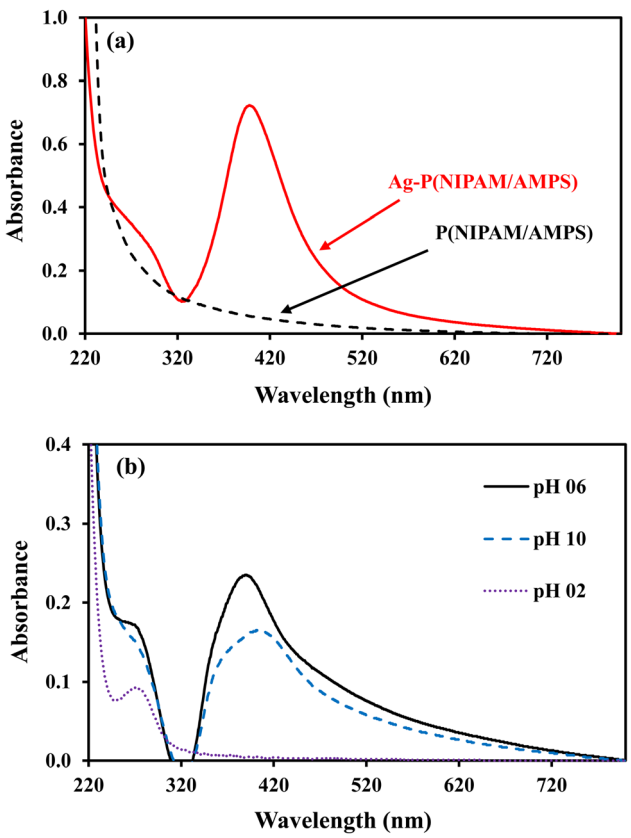

Fig. 4 (a) UV-visible spectra of p(NIPAM/AMPS) and Ag–p(NIPAM/AMPS) (b) pH effect on surface plasmon of Ag–p(NIPAM/AMPS).

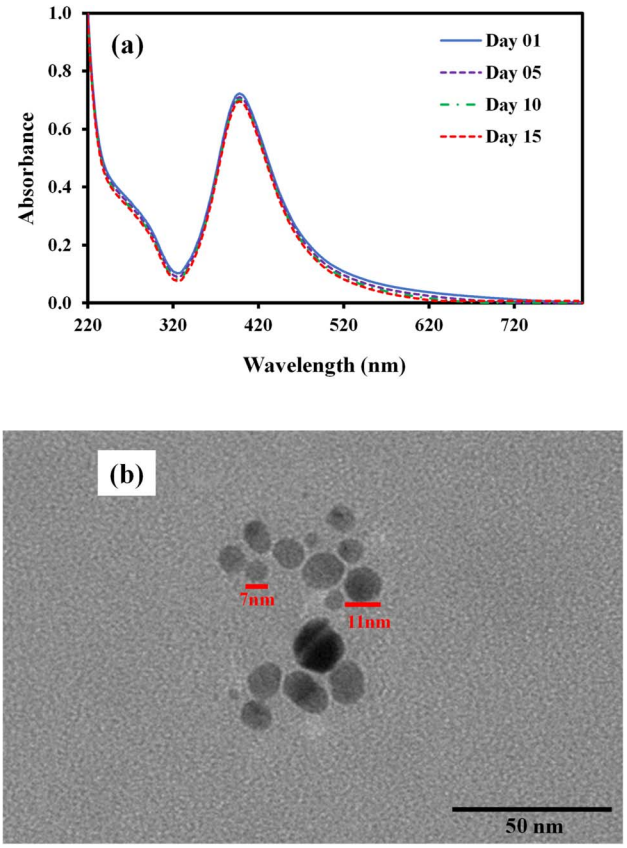

Fig. 5 (a) UV-visible spectra of Ag–p(NIPAM/AMPS) as a function of time for 15 days (b) TEM image of Ag–p(NIPAM/AMPS).

was observed. The decrease in weight loss can be associated to the presence of AgNPs.[35] So, this thermal study showed that 15% AgNPs–MG was consisting of Ag nanoparticles. In addition to providing an idea about the amount of AgNPs in AgNPs–MG, this thermal study showed that AgNPs–MG are thermally stable below 200 °C and can be applied for different applications below this temperature.

The prepared BMG and AgNPs–MG contain NIPAM and AMPS which are thermo- and pH responsive, respectively. Therefore, these microgels were found to response both the temperature and pH of the medium. This responsive behavior was studied by DLLS. The diameters of the microgel particles were determined as a function of pH and temperature as illustrated by Fig. 3(a) and (b), respectively. The acidic and basic mediums were prepared by using concentrated solutions of HCl and NaOH, respectively. Fig. 3(a) shows that the particle size of microgels enlarged gradually with enhancing the pH of the medium. The sulfonic acid groups of AMPS units remain protonated in highly acidic medium which makes the microgel particles hydrophobic with globular arrangement of polymer chains. As the pH increases, the deprotonated of sulfonic acid group occurs leading to the formation of SO_3^- ions. The electrostatic repulsion is created between the SO_3^- units on polymer chains which causes the expansion of polymer chains. The amid groups of AMPS units are exposed to surrounding water molecules with the expansion of polymer chains and water gets absorbed in the microgel network.[36] The expansion of polymer chains and absorption of water molecules collectively increase the particle size of microgels.[37] The deprotonation of AMPS groups is completed at a certain pH and then further increase in pH imparts no effect on the particle size. The process of swelling of microgel particles has been illustrated schematically in Fig. 3(a) which shows enlargement in the microgel particle size with deprotonation and polymer chain extension with a corresponding increase in pH of the medium.

Thermo-responsive behavior of the prepared microgels was examined in the temperature range of 20 to 60 °C. By increasing the temperature, the hydrodynamic diameter of microgels was decreased as shown in Fig. 3(b). At low temperature condition, amide and sulfonic acid groups form hydrogen bonds with water molecules and large amount of water remains encapsulated in microgel network which in turn increases the size of microgel particles. However, the increase in temperature raises the average kinetic energy of the water molecules which leads to breakdown of hydrogen bonding between microgel network and water molecules.[38] The water molecules rushed out from the microgel network and size of the microgel particles is decreased as illustrated in Fig. 3(b). The process of decrease of size of microgel particles has been illustrated schematically in Fig. 3(b) which shows the gradual decrease in particle size with the increase in temperature of medium which in turn causes the removal of water from microgel network due to breakdown of hydrogen bonding between the water molecules and functional groups of microgel.

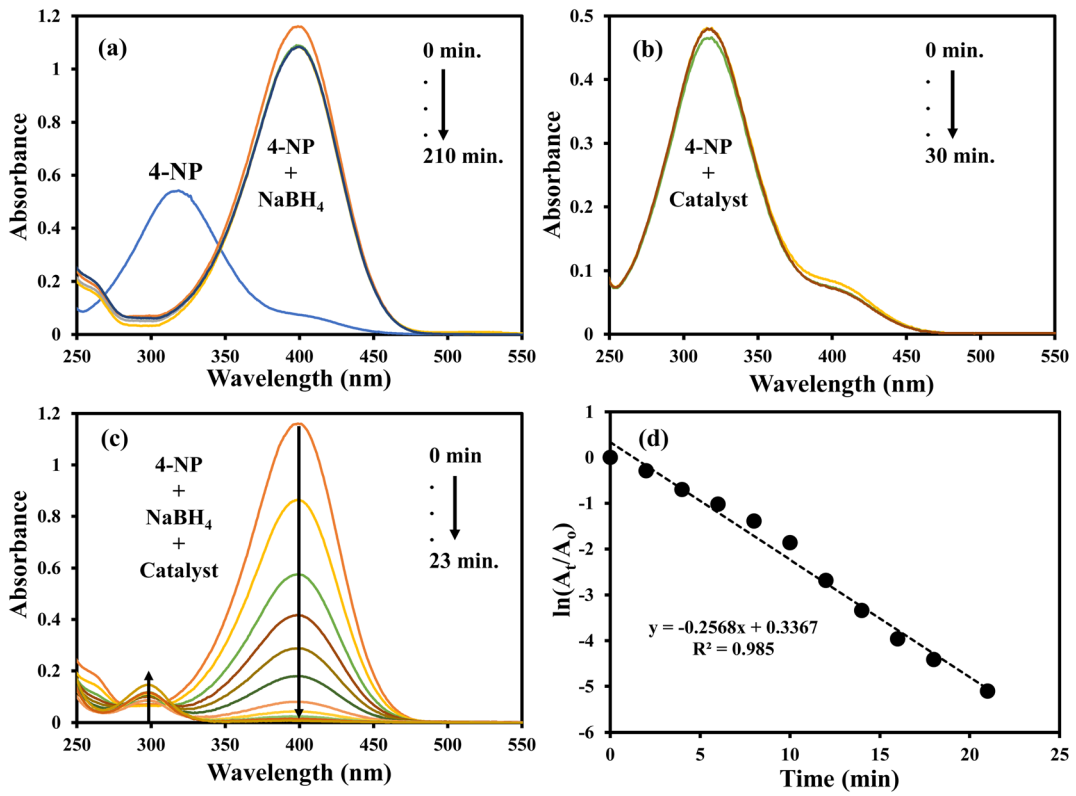

Fig. 6 UV-visible spectra of (a) 4-NP and 4-NP + $NaBH_4$, (b) 4-NP + Ag–p(NIPAM/AMPS), (c) 4-NP + Ag–p(NIPAM/AMPS) + $NaBH_4$, (d) plot of $\ln(A_t/A_o)$ *vs.* time.

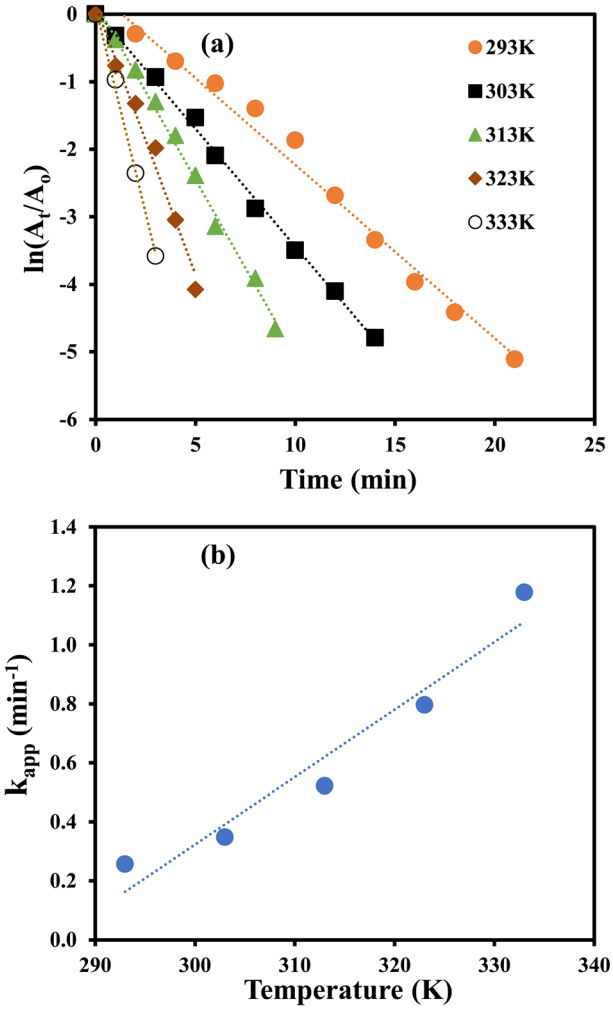

Fig. 7 (a) Kinetic study for reduction of 4-NP at different temperatures. (b) Apparent rate constant *vs.* temperature for catalytic reduction of 4-NP.

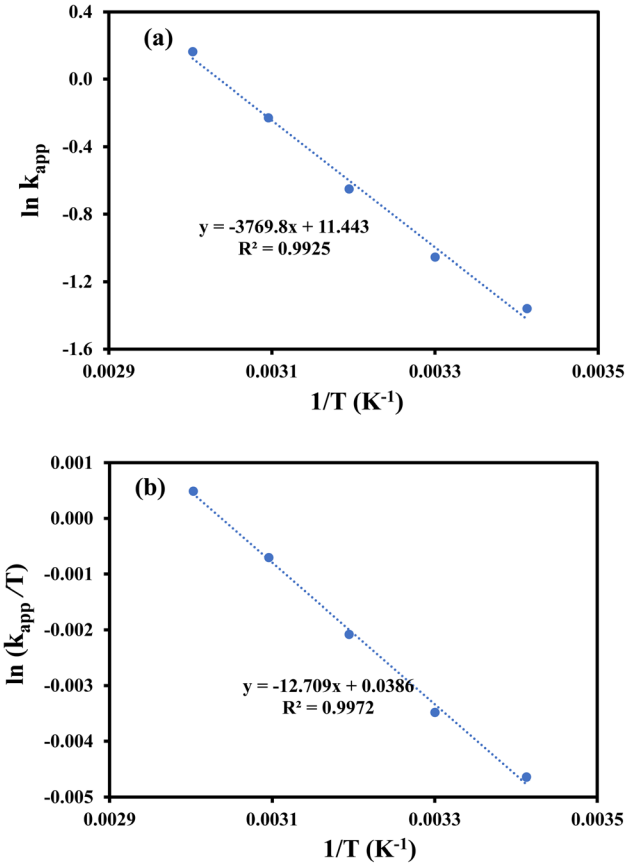

Fig. 8 (a) Plot of ln k_{app} *vs.* 1/*T* for calculating activation energy of 4-NP, (b) plot of ln(k_{app}/*T*) *vs.* 1/*T* for calculating entropy and enthalpy of activation.

Silver nanoparticles fabricated within microgel absorb blue light and reflect green and red lights which are mixed to give yellow color to microgel containing AgNPs. The dipole moment of AgNP's is responsible for the absorption peak around 400 nm for AgNP's. The BMG particles do not contain AgNPs and therefore do not show any absorption while AgNPs–MG exhibit absorption peak around 400 nm as depicted from Fig. 4(a). The surface polarization and refractive index of medium are the two factors which determine the intensity of plasmon resonance nanoparticles and its frequency.[39] Both the surface polarization and refractive index of medium are the function of pH of the medium. Therefore, UV-Vis absorption of AgNPs–MG was studied at pH 2, 6, and 10 and the results have been represented in Fig. 4(b). It was observed that with the increase in pH surface plasmon wavelength (λ_{spr}) of AgNP's was red shifted from 393 to 406 nm. The change in the surface polarization and refractive index of medium as a function of pH is responsible for this shift in λ_{spr} towards longer wavelength. A change in the pH of the medium causes swelling/deswelling of microgel particles and induce a change in the local refractive on the surface of AgNP's.[40] In the basic medium (high pH), the sulfonic acid groups remain deprotonated and hence carry negative charges. The electrostatic repulsion is created between the negatively charged sulfonic acid groups and causes the microgel to swell. In swollen microgel, the distance between AgNP's is increased and electrons oscillate slowly showing plasmon resonance at longer wavelength. In acidic medium (low pH), the sulfonic acid is protonated and causes deswelling of the microgel and the distance between AgNPs is decreased resulting a blue shift (decrease) in λ_{spr}. At highly acidic pH of the medium the AgNPs move out of microgel and aggregate forming large particles. The size of these aggregated particles does not lie in the nano range so no characteristic plasmon resonance band appeared[15] as can be seen from the spectrum at pH = 2 in Fig. 4 (b). In order to find the stability of AgNPs fabricated in our prepared MG, the prepared AgNPs–MG were stored in airtight containers and their UV-Vis spectra were recorded as a function of time for fifteen days as shown in Fig. 5(a). The results revealed that no observable changes appeared in the UV-Vis spectra of AgNPs–MG even after 15 days and hence demonstrating that AgNPs were quite stable in our reported MG. The morphology and stability of AgNPs fabricated MG were further examined with TEM. Fig. 5(b) represents the TEM image of AgNPs–MG which demonstrate that most of the AgNPs were having diameters in

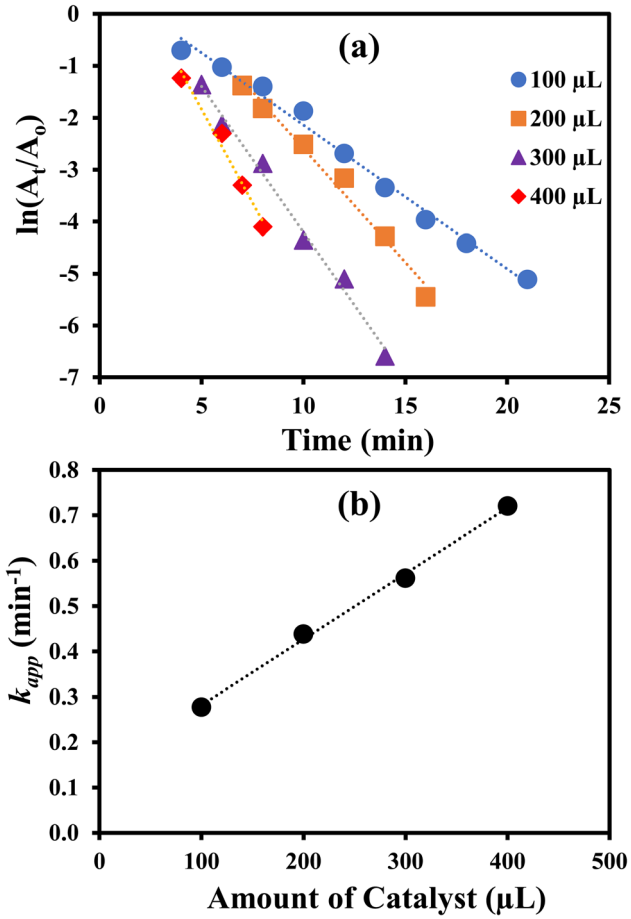

Fig. 9 (a) Plot of $\ln(A_t/A_o)$ *vs.* time for the reduction of 4-NP with different amounts of catalyst. (b) Plot of apparent rate constant *vs.* amount of catalyst.

the range of 7–11 nm and no aggregation of AgNPs was observed in MG. The narrow size distribution AgNPs and absence of aggregation demonstrates that MG has acted as an effective reactor and stabilizer for AgNPs.

3.2 Catalytic reduction of water pollutants

The nitroaromatic compounds were reduced using AgNPs–MG as a catalyst. Reduction of 2-nitroaniline (2-NA), 2-nitrophenol (2-NP), and 4-nitrophenol (4-NP) with sodium borohydride ($NaBH_4$) were chosen as representative nitroaromatic compounds reduction reactions to test the catalytic potential of the prepared AgNPs–MG. These nitrocompounds were selected to multiple reasons. Firstly, these nitrocompounds are considered as pollutants. For example, according to Agency for Toxic Substances and Disease Registry of the United States, 4-NP causes inflammation and irritation of the skin, eyes, and respiratory tract.[41] Secondly, reduction of these nitrocompounds are intermediate steps in pharmaceutical and coloring industries. For example, reduction of 4-NP to produce 4-AP is involved in the formation of antipyretic and analgesic medicines such as paracetamol, acetanilide, and phenacetin while the reduction 2-NP and 2-NA are involved in the synthesis of dyes and pigments.[42] Thirdly, due to kinetic barrier between BH_4^- and the nitrocompounds, their reduction reactions take at negligible rates in the absence of a suitable catalyst, and it makes these reactions as ideal reactions to determine the catalytic activity. Fourthly, the both the reactants and products of these reactions can be monitored with commonly used technique UV-Vis spectroscopy. Reduction of these nitroaromatic compounds by using $NaBH_4$ as reducing agent is not feasible due to kinetic barrier between BH_4^- and 4-NP.[3] To overwhelm this kinetic barrier AgNPs can act as electron relay system. Therefore, we used our prepared AgNPs–MG as catalyst in the reduction of considered nitroaromatic compounds. Since the reactants and products of these reactions are UV-visible active, these catalytic reduction reactions were assessed using UV-visible spectroscopy. The aqueous solution of 4-NP exhibits absorption band at 317 nm and is red-shifted to 400 nm when $NaBH_4$ added in it. This happens due to the formation of nitrophenolate ions. These ions are stabilized by delocalization in aromatic ring. The absorption peak of nitrophenolate ion remains stable in the absence of catalyst as shown in Fig. 6(a). On the other hand, the aqueous solution of 4-NP in the existence of AgNPs–MG also showed a stable absorption peak at 317 nm as shown in Fig. 6(b) and hence representing that AgNPs–MG cannot act as reducing agent but acts as catalyst. Fig. 6(c) represents the decrease in absorbance of 4- nitrophenolate ion at 400 nm due to its reduction with $NaBH_4$ which was catalyzed with AgNPs–MG. A new absorption peak at 298 nm confirms the formation of 4-AP. In this reaction, the reducing agent was used in large excess so pseudo first order kinetics was applied to compute the apparent rate constant (k_{app}) of the reaction[43] as shown in Fig. 6(d). The k_{app} for the catalytic reduction of 4-NP using 100 times surplus amount of $NaBH_4$ was calculated to be 25.68×10^{-2} min^{-1} at 293 K.

The catalytic reduction of 4-NP was monitored at 293, 303, 313, 323 and 333 K to compute the thermodynamic parameters. At each temperature, k_{app} was computed by pseudo first order kinetics as illustrated in Fig. 7(a) and it was noted that the value of k_{app} was increased with increasing temperature as illustrated from Fig. 7(b). This observation reveals that catalytic reduction of 4-NP was an endothermic reaction. This increase in k_{app} as a function of temperature can be associated to the increase in the collision frequency of the reactants owing to an enhancement in the average kinetic energy of the reactants.

The thermodynamic parameters were computed by fitting the Arrhenius and Eyring equations (eqn (1) and (2)) on the experimental data.

$$\ln k_{app} = \ln A - (E_a/RT) \quad (1)$$

$$\ln(k_{app}/T) = \ln(k_b/h) + \Delta S^{\#}/R - \Delta H^{\#}/RT \quad (2)$$

where, k_{app} is apparent rate constant in min^{-1}, A is Arrhenius constant in min^{-1}, E_a is activation energy in J mol^{-1}, R is the general gas constant and its value is 8.314 J mol^{-1} K^{-1}, T is temperature in K, $\Delta S^{\#}$ is Activation entropy change (J mol^{-1} K^{-1}), $\Delta H^{\#}$ is activation enthalpy change (J mol^{-1}), h is Planck's constant (6.626×10^{-34} J s) and k_b is Boltzmann constant (1.38

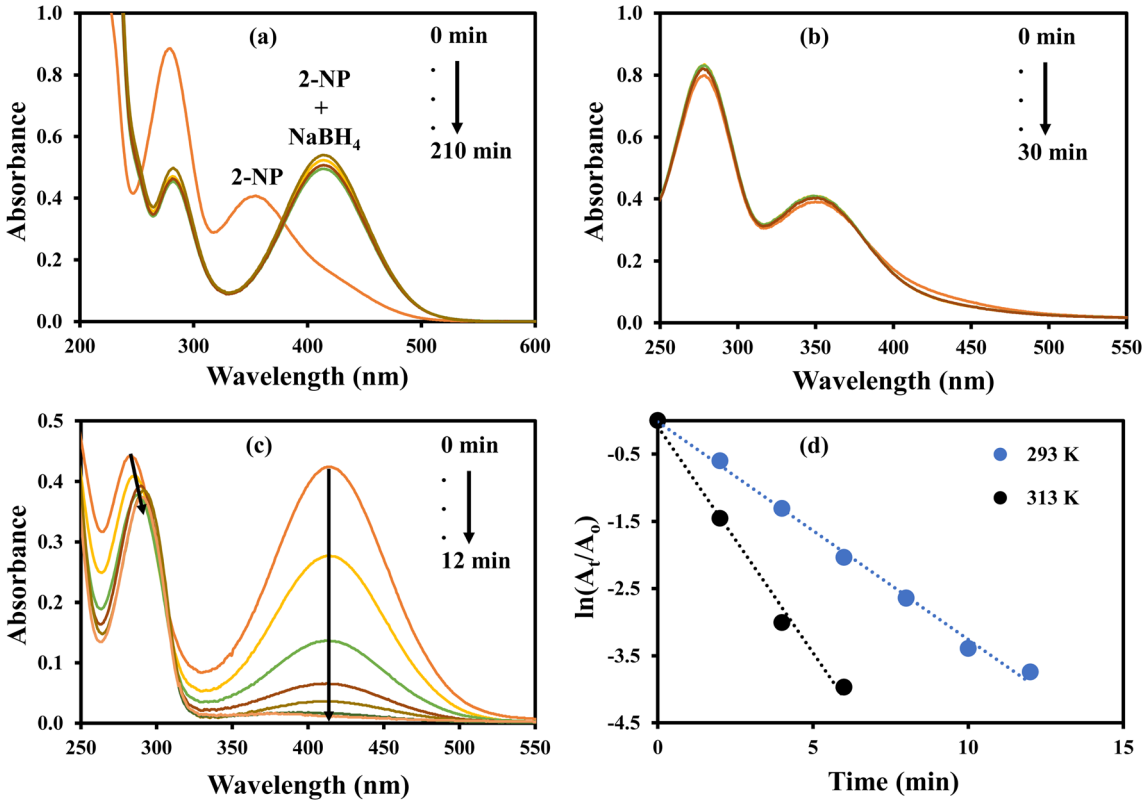

Fig. 10 UV-visible spectra of (a) 2-NP and 2-NP + $NaBH_4$, (b) 2-NP + Ag–p(NIPAM/AMPS), (c) 2-NP + Ag–p(NIPAM/AMPS) + $NaBH_4$, (d) plots of $\ln(A_t/A_o)$ *vs.* time.

$\times 10^{-23}$ J K^{-1}). The value of E_a was computed from the slope of the plot of $\ln k_{app}$ *vs.* $1/T$ (Fig. 8(a)) and found to be 31.34 kJ mol^{-1}. The values of $\Delta S^{\#}$ and $\Delta H^{\#}$ were computed from the slope and intercept of the graph of $\ln k_{app}/T$ *vs.* $1/T$ as shown in Fig. 8(b) and were found as −158.474 J mol^{-1} K^{-1} and 28.746 kJ mol^{-1} and, respectively. The positive value of $\Delta H^{\#}$ of activated complex indicated that formation of activated complex in the reduction process was endothermic in nature. On the other hand, the negative value $\Delta S^{\#}$ of activated depicted that entropy of the system was decreased. This observation reveals that the random dispersion of the molecules was restricted due to the adsorption of reactant molecules on AgNPs and therefore, entropy of the system is decreased as activated complex is formed. Using the values of $\Delta H^{\#}$, $\Delta S^{\#}$ and temperature, the values of $\Delta G^{\#}$ were computed for each temperature and found to increase from 46.5 to 52.8 kJ mol^{-1} with a corresponding increase in temperature from 293 to 333 K. These positive values of $\Delta G^{\#}$ and their increase with temperature represents that the reaction was non-spontaneous and endothermic. The reduction of 4-nitrophenol was also carried out with 100 μL, 200 μL, 300 μL and 400 μL of AgNPs–MG as catalyst. The k_{app} was computed from the slopes of the plots of pseudo first order kinetics as shown in Fig. 9(a) and it was found to vary linearly with the amount of catalyst as shown in Fig. 9(b). This increase in k_{app} is associated to increase in the surface area of catalyst available for adsorption of reactant which is increased due to increase in the amount of catalyst.[44]

The aqueous solution of 2-NP showed the absorption peaks at 278 and 315 nm and these peaks were transferred to 283 and 413 nm upon the addition of $NaBH_4$ and no considerable decrease was detected in the absorption intensity for long time as shown in Fig. 10(a). A change in color from light yellow to bright yellow was also observed parallel to the shift in absorption peaks. This change in color and absorption peaks appear due to formation of 2-nitrophenolate ion by the reaction of 2-NP and $NaBH_4$. No variation in the color of 2-NP solution and no disturbance in the intensity and position of absorption peaks were observed when only AgNPs–MG was added in the aqueous solution of 2-NP as shown in Fig. 10(b). The results demonstrated that AgNPs–MG cannot act as reducing while $NaBH_4$ acts as a reducing agent but has not enough potential to reduce the 2-NP.[45] The formation of 2-aminophenol from 2-nitrophenolate ion with $NaBH_4$ is kinetically hindered. To overcome this kinetic energy barrier, AgNPs–MG was added as catalyst and reduction of 2-nitrophenolate ion was occurred as demonstrated by the diminution in the absorption band at 415 nm and red shift in the absorption band at 283 nm as shown in Fig. 10(c). The k_{app} was computed using pseudo-first order kinetics. The pseudo first order plots at 20 and 40 °C are shown in Fig. 10(d). The value of k_{app} was enhanced from 32.4 $\times$ 10^{-2} min^{-1} to 67.3 $\times$ 10^{-2} min^{-1} with the increase in temperature from 20 to 40 °C implying that the reaction was

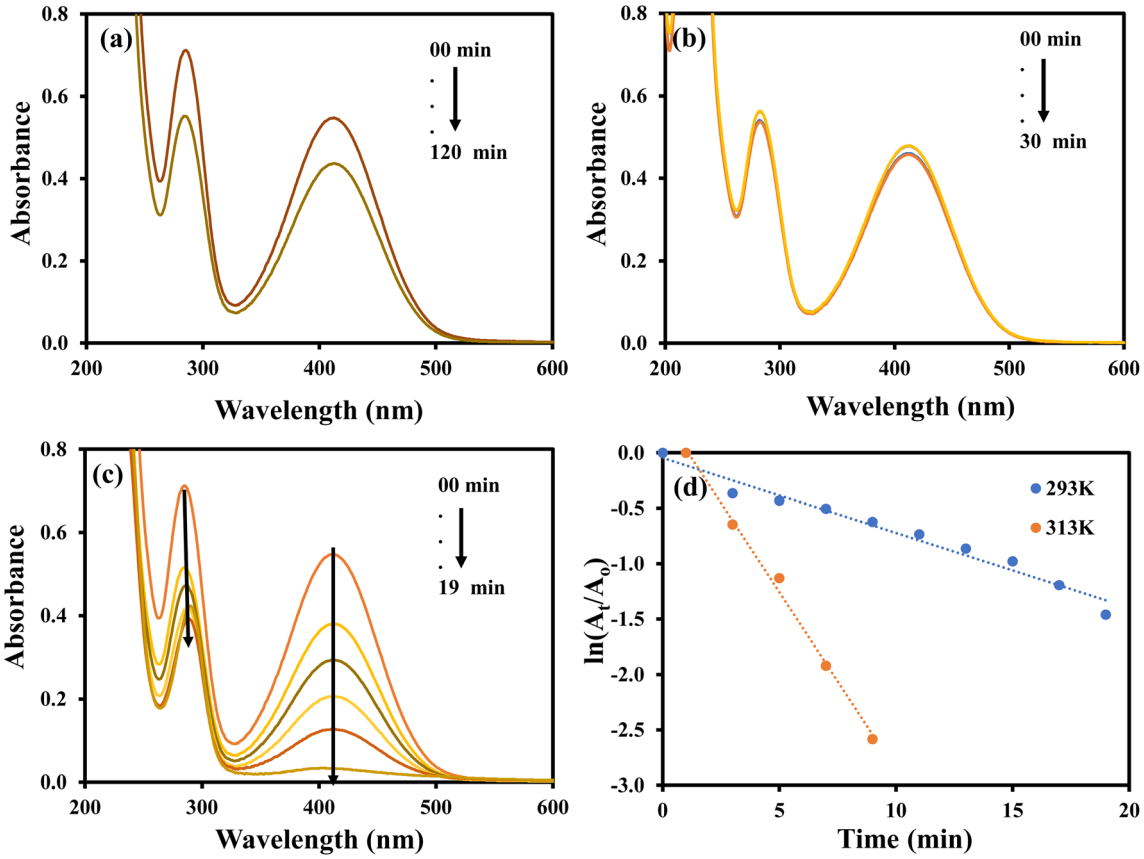

Fig. 11 UV-visible spectra for the reduction of 2-nitroaniline (a) with $NaBH_4$ in the absence of catalyst. (b) In the presence of catalyst without $NaBH_4$. (c) With $NaBH_4$ in the presence of catalyst. (d) Plot of $\ln(A_t/A_o)$ *vs.* time. Reaction conditions: 1 mM 2-NA = 40 mL, 0.1 M $NaBH_4$ = 1.5 g, catalyst = 100 μL.

endothermic. Activation energy was calculated by using Arrhenius equation and found as 27.868 kJ mol^{-1}.

Fig. 11 shows the results for the reduction of 2-NA. The aqueous solution of 2-NA showed characteristic absorption bands at 287 and 412 nm and a slight decline in the absorption intensity was noted upon the addition of $NaBH_4$ even after long contact time as shown in Fig. 11(a). This indicated that $NaBH_4$ was not having enough potential to reduce 2-NA owing to large kinetic barrier. Fig. 11(b) represents the UV visible spectra of the aqueous solution of 2-NA added with AgNPs–MG and shows a very slight decline in the absorption intensity in first few minutes of contact time and no more decline in the absorption strength was observed later. This observation can be associated to the little adsorption of 2-NA on the surface of AgNPs–MG which is also a prerequisite for a catalytic reaction. Fig. 11(c) shows the reduction of 2-NA with $NaBH_4$ and catalyzed by AgNPs–MG. The absorption peak at 412 nm was gradually disappeared and the peak around 287 nm was also reduced. This observation confirmed that 2-NA was successfully reduced to 2-phenyldiammine (2-PDA).[46] The reaction was carried out at 293 and 313 K. The k_{app} was computed with pseudo first kinetics and found 6.76×10^{-2} min^{-1} and 32.21×10^{-2} min^{-1} at 293 and 313 K, respectively. Fig. 11(d) shows the plots of pseudo first kinetics for the catalytic reduction of 2-NA at 293 and 313 K. The increased value of k_{app} at higher temperature showed that the reduction of 2-NA was an endothermic process. The E_a was calculated by Arrhenius equation and found to be 59.5 kJ mol^{-1}.

3.3 Catalytic degradation of dyes

The catalytic potential of AgNPs–MG was further explored in the decolorization of methylene blue (MB), methyl orange (MO), and eosin Y (EY).

The aqueous solution of MO gives maximum absorption band at 464 nm. The MO can be reduced with $NaBH_4$, but this reduction is almost negligible in the absence of a suitable catalysts due to large kinetic barrier among the electron donor and accepter of this process. Therefore, a negligible decline in the absorbance of the aqueous solution of MO was observed when it was treated with $NaBH_4$ as shown in Fig. 12(a). Similarly, a small decline in the absorbance of the aqueous solution of MO was observed upon its interaction with AgNPs–MG as shown in Fig. 12(b). Since, AgNPs–MG has no electron donating agent so it cannot reduce MO and the drop in the absorbance of the aqueous solution of MO can be observed due to little adsorption of MO on AgNPs–MG which is a prerequisite of catalysis process. Similar observations have already been reported.[47] Fig. 12(c) shows the reduction of MO with $NaBH_4$ and catalyzed by AgNPs–MG. The absorption peak at 464 nm was

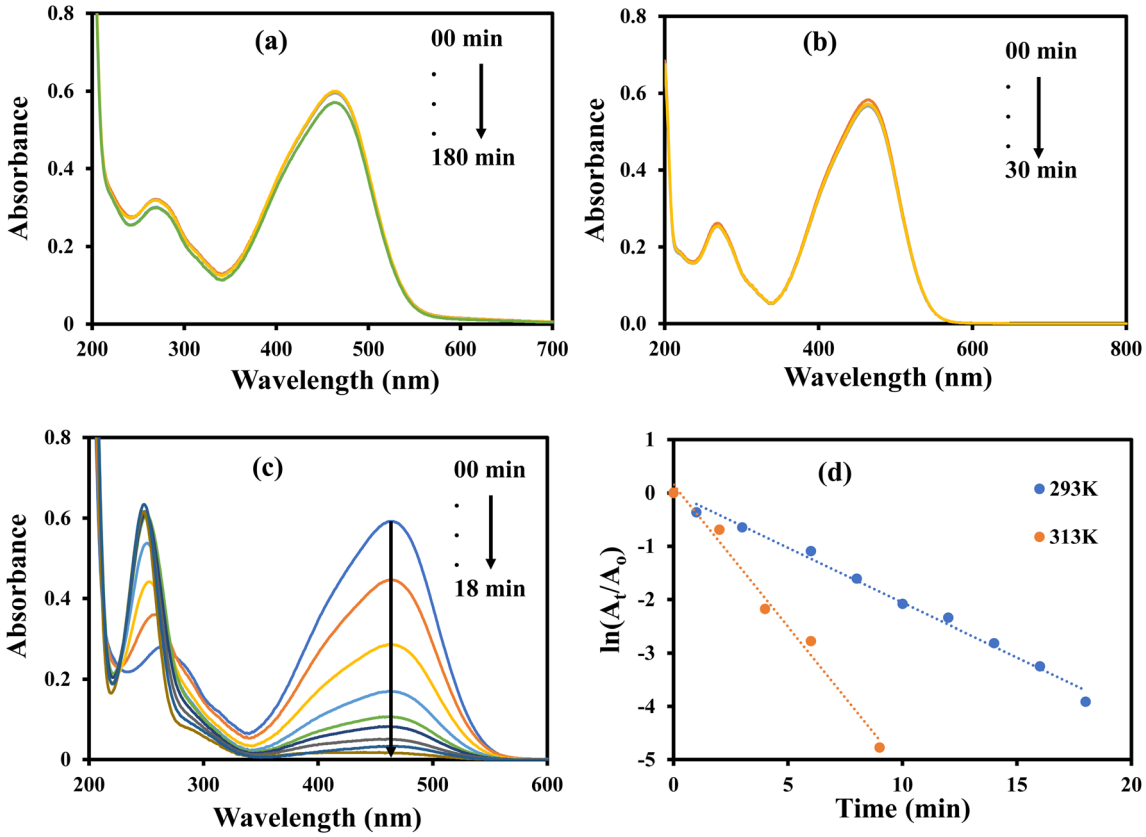

Fig. 12 UV-visible spectra for the reduction of methyl orange (a) with $NaBH_4$ in the absence of catalyst. (b) In the presence of catalyst without $NaBH_4$. (c) With $NaBH_4$ in the presence of catalyst. (d) Plot of $\ln(A_t/A_o)$ *vs.* time. Reaction conditions: 4×10^{-4} M methyl orange = 40 mL, 0.04 M $NaBH_4$ = 0.242 g, catalyst = 400 μL.

gradually disappeared and confirmed that MO was successfully reduced to colorless reagents. The reaction was carried out at 293 and 313 K. The k_{app} was computed with pseudo first kinetics and found 20.5×10^{-2} min^{-1} and 53.2×10^{-2} min^{-1} at 293 and 313 K, respectively. Fig. 12(d) shows the plots of pseudo first kinetics for the catalytic reduction of MO at 293 and 313 K. The increased value of k_{app} at higher temperature showed that the reduction of MO was an endothermic process. The E_a was calculated by Arrhenius equation and was found as 36.26 kJ mol^{-1}.

The aqueous solution of MB gives highest absorption peak at 664 nm. The MB can be reduced with $NaBH_4$, but this reduction is almost negligible in the absence of a suitable catalysts due to large kinetic barrier among the electron donor and accepter of this process. Therefore, a negligible decrease in the absorbance of the aqueous solution of MB was observed when it was treated with $NaBH_4$ as shown in Fig. 13(a). Similarly, a small decline in the absorbance of the aqueous solution of MB was observed upon its interaction with AgNPs–MG as shown in Fig. 13(b). Since, AgNPs–MG has no electron donating agent so it cannot reduce MB and the decrease in the absorbance of the aqueous solution of MB can be associated to little adsorption of MB on AgNPs–MG which is a prerequisite of catalysis process. Similar observations have already been reported.[18] Fig. 13(c) shows the reduction of MB with $NaBH_4$ and catalyzed by AgNPs–MG. The absorption peak at 664 nm was gradually disappeared and confirmed that MB was successfully reduced to colorless reagents.[48] The reaction was carried out at 293 and 313 K. The k_{app} was computed with pseudo first kinetics and found 9.4×10^{-2} min^{-1} and 34.6×10^{-2} min^{-1} at 293 and 313 K, respectively. Fig. 13(d) shows the plots of pseudo first kinetics for the catalytic reduction of MB at 293 and 313 K. The increased value of k_{app} at higher temperature showed that the reduction of MB was an endothermic process. The E_a was calculated by Arrhenius equation and was found as 49.65 kJ mol^{-1}.

The aqueous solution of EY gives highest absorption peak at 516 nm.[49] The EY can be reduced with $NaBH_4$, but this reduction is almost negligible in the absence of a suitable catalysts due to large kinetic barrier among the electron donor and accepter of this process. Therefore, a negligible decrease in the absorbance of the aqueous solution of EY was observed when it was treated with $NaBH_4$ as shown in Fig. 14(a). Similarly, a small decrease in the absorbance of the aqueous solution of EY was observed upon its interaction with AgNPs–MG as shown in Fig. 14(b). Since, AgNPs–MG has no electron donating agent so it cannot reduce EY and the decrease in the absorbance of the aqueous solution of EY can be associated to little adsorption of EY on AgNPs–MG which is a prerequisite of catalysis process. Similar

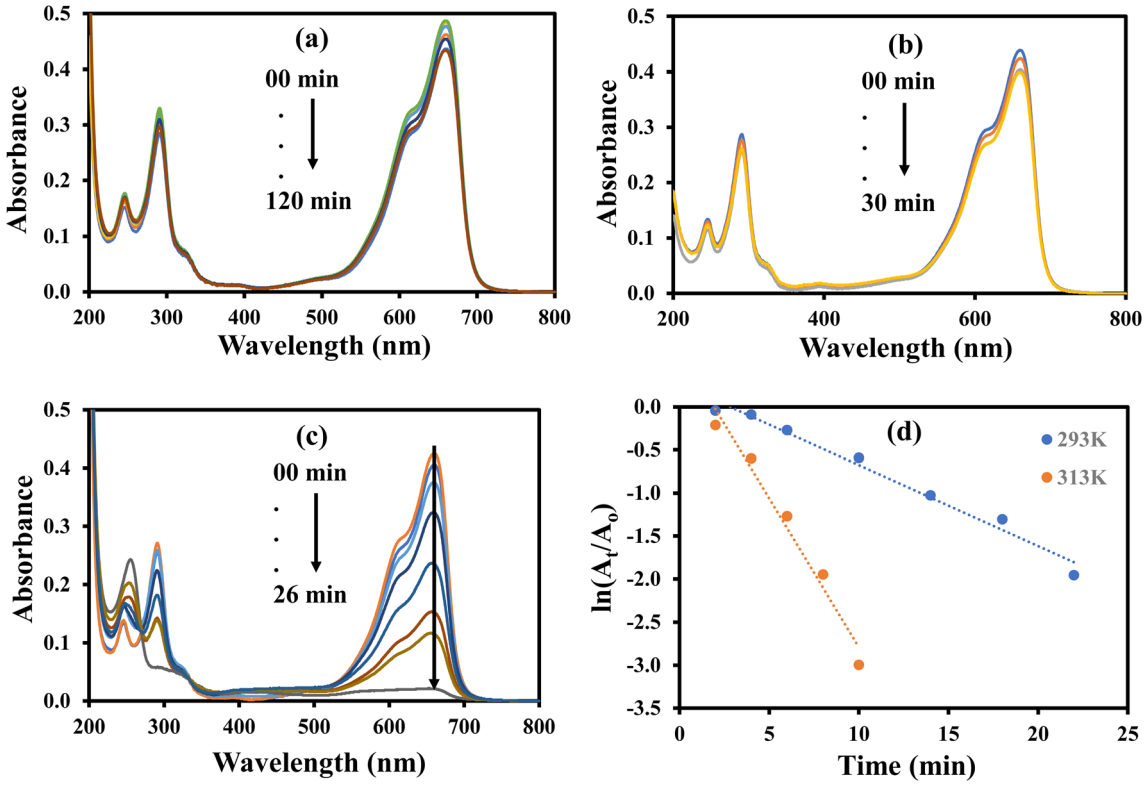

Fig. 13 UV-visible spectra for the reduction of methylene blue (a) with $NaBH_4$ in the absence of catalyst. (b) In the presence of catalyst without $NaBH_4$. (c) With $NaBH_4$ in the presence of catalyst. (d) Plot of $\ln(A_t/A_o)$ *vs.* time. Reaction conditions: 1.6×10^{-4} M methylene blue = 40 mL, 0.04 M $NaBH_4$ = 0.0968 g, catalyst = 400 μL.

observations have already been reported.[18] Fig. 14(c) shows the reduction of EY with $NaBH_4$ and catalyzed by AgNPs–MG. The absorption peak at 664 nm was gradually disappeared and confirmed that EY was successfully reduced to colorless reagents.[42] The reaction was carried out at 293 and 313 K. The k_{app} was computed with pseudo first kinetics and found 10.77×10^{-2} min^{-1} and 23.63×10^{-2} min^{-1} at 293 and 313 K, respectively. Fig. 14(d) shows the plots of pseudo first kinetics for the catalytic reduction of EY at 293 and 313 K. The increased value of k_{app} at higher temperature showed that the reduction of EY was an endothermic process. The E_a was calculated by Arrhenius equation and was found as 29.95 kJ mol^{-1}. In case of the catalytic reduction of all the three dyes studied in this work, it was observed that their absorbance was reduced in visible region with a corresponding enhancement of the absorbance in the UV region. This observation indicates that the dyes have been converted from their colored and toxic oxidized form to transparent and less toxic reduced forms.[50]

Table 1 represents the comparison of the results of catalytic of present work with those already reported in literature in terms of k_{app}. As it can be seen from Table 1, the catalytic activity of our prepared Ag–p(NIPAM/AMPS) catalyst in the reduction of nitrocompounds and dyes much better than many other catalysts. So, in this work a catalyst with improved efficiency has been prepared.

3.4 Colorimetric sensing of H_2O_2

AgNPs–MG show absorption peak around 400 nm (yellow color) and can be used as colorimetric sensor for biochemicals which can affect its absorption intensity/peak position. AgNPs are oxidized upon interaction with H_2O_2. The conversion of Ag to Ag^+ ions is responsible for the lowering of typical absorption peak of AgNPs–MG.[18] Therefore, synthesized AgNPs–MG was tested as chemical sensor for H_2O_2. As expected, a decrease in the absorption intensity at wavelength corresponding to SPR of AgNPs was observed upon the interaction of AgNPs–MG with H_2O_2 as shown in Fig. 15(a). In addition, the yellow color of the mixture of AgNPs–MG and H_2O_2 was also faded with time. For qualitative analysis, the decrease in the absorption intensity at the wavelength corresponding to the SPR of AgNPs was observed as function of concentration of H_2O_2. A linear increase in the magnitude of the percentage change in the absorption intensity was observed as illustrated in Fig. 15(b). These results also demonstrated that our prepared AgNPs–MG was able to detect H_2O_2 with concentration as low as 50 μM when treated in a volume ratio of 7 : 1. According to the above-mentioned results, the change in absorption strength of SPR of AgNPs can be used as a sensitive signal for the colorimetric detection of H_2O_2.

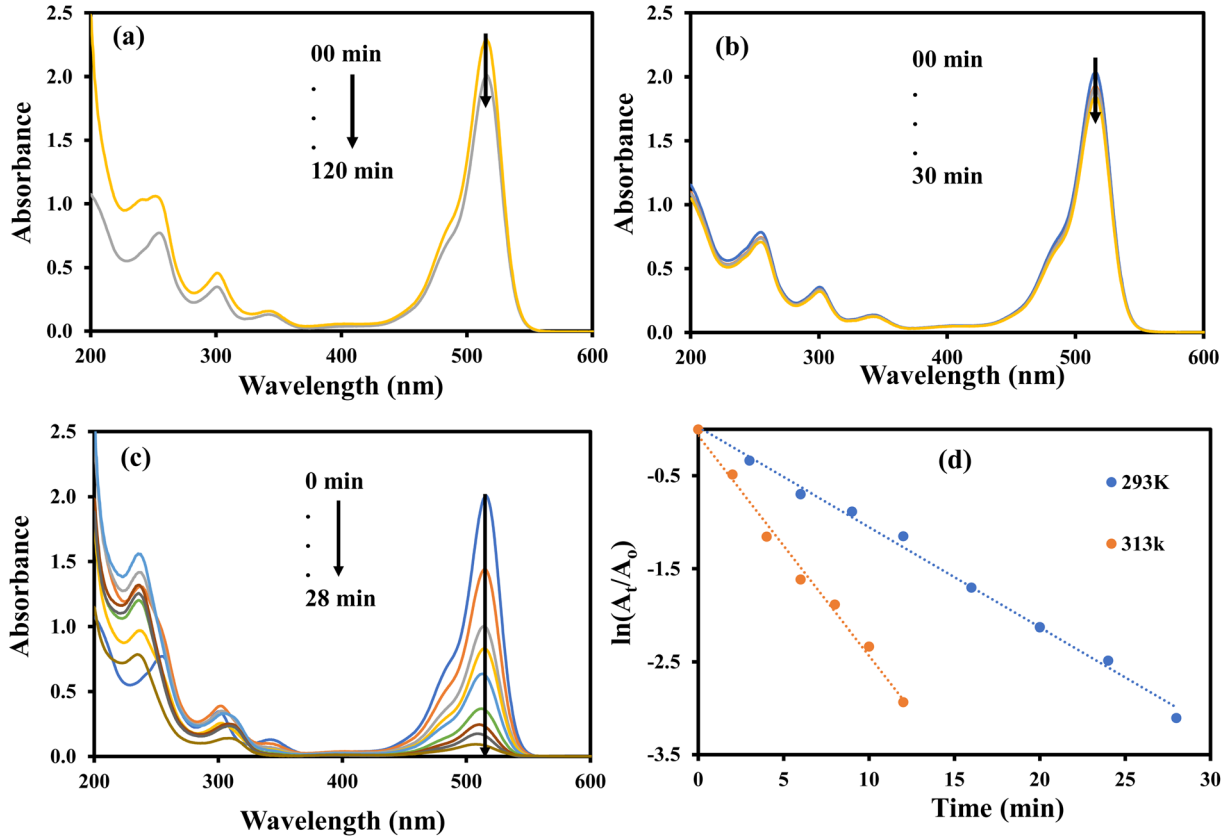

Fig. 14 UV-visible spectra for the reduction of eosin Y (a) with $NaBH_4$ in the absence of catalyst. (b) In the presence of catalyst without $NaBH_4$. (c) With $NaBH_4$ in the presence of catalyst. (d) Plot of $\ln(A_t/A_o)$ *vs.* time. Reaction conditions: 4×10^{-4} M eosin Y = 40 mL, 0.04 M $NaBH_4$ = 0.242 g, catalyst = 400 μL.

Table 1 Comparison of catalytic activity of our prepared Ag–p(NIPAM/AMPS) catalyst with those reported in literature in terms of apparent rate constant (k_{app}) for the catalytic reduction of 4-nitrophenol (4-NP), 2-nitrophenol (2-NP), methyl orange (MO), methylene blue (MB), and eosin Y (EY)

S. no.	Reactant	Catalyst	k_{app} (min^{-1})	Reference
1	4-NP	Ag@conjugated microporous polymer	59.7×10^{-2}	51
2	4-NP	Ag–SiO_2 xerogel	88×10^{-2}	52
3	4-NP	Ag–Al_2O_3 xerogel	71.4×10^{-2}	52
4	4-NP	Ag–p(NIPAM/AMPS)	117×10^{-2}	Present work
5	2-NP	Ag@conjugated microporous polymer	6.35×10^{-2}	51
6	2-NP	Poly(acrylic acid)–AgNPs	14.62×10^{-2}	23
7	2-NP	Graphene oxide/hydroapatite–AgNPs	8.98×10^{-2}	53
8	2-NP	Ag–p(NIPAM/AMPS)	32.4×10^{-2}	Present work
9	2-NA	GO–CoNPs	6.0×10^{-2}	
10	2-NA	Ag–p(NIPAM/AMPS)	6.76×10^{-2}	Present work
11	MO	Glutathione–AgNPs	9.2×10^{-2}	54
12	MO	Ag–p(NIPAM/AMPS)	53.2×10^{-2}	Present work
13	MB	Au/TiO_2	15.6×10^{-2}	55
14	MB	Ag–p(NIPAM/AMPS)	34.6×10^{-2}	Present work
15	EY	AuNP–nodiflora	12.46×10^{-2}	56
16	EY	Ag–p(NIPAM/AMPS)	23.63×10^{-2}	Present work

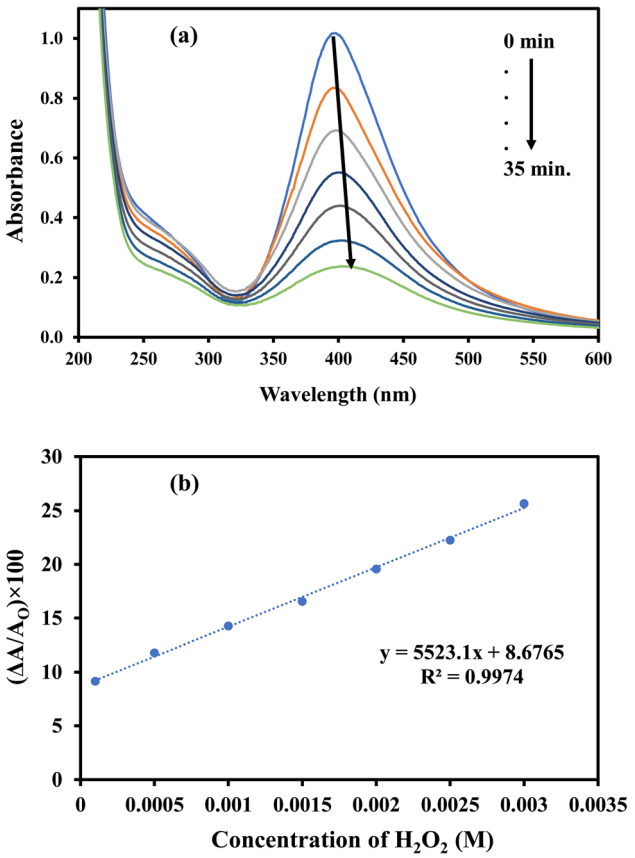

Fig. 15 (a) UV-Vis spectra of Ag–p(NIPAM/AMPS) containing H_2O_2, (b) calibration curve for the detection of H_2O_2 using Ag–p(NIPAM/AMPS).

4. Conclusions

In this study, bare p(NIPAM-*co*-AMPS) microgel (BMG) was synthesized by free radical polymerization successfully and used as reactor for the *in situ* fabrication of AgNPs by chemical reduction method. The FTIR results identified the formation of BMG by polymerization reaction and the presence of corresponding functional groups. The XRD analysis showed that BMG was amorphous however upon the fabrication of AgNPs crystalline behavior was observed supporting the presence of AgNPs within MG networks. The DLS studies confirmed the particulate nature of BMG and AgNPs–MG, and the particle size was found to be increased with increase in pH and decreased with increase in temperature. TGA curve ensured thermal stability of both the BMG and AgNPs–MG up to 350 °C. The reduction of 4-NP, 2-NP, 2-NA, EY, MO, and MB showed that the prepared AgNPs–MG could be used as effective catalysts. The catalytic reduction reactions of all the subjected reagents were found to be endothermic. The prepared AgNPs–MG showed better catalytic performance for 4-NP as compared to other nitro compounds with k_{app} value of 1.1778 min^{-1}. While in case of dyes the catalytic performance of AgNPs–MG was found better for MO as compared to other dyes with maximum value of k_{app} equal to 0.532 min^{-1}. In addition to act as a catalyst for different water pollutants, the prepared AgNPs–MG have also shown working potential as a biosensor for H_2O_2 with its concentration as low as 50 μM.

Conflicts of interest

The authors declare that they have no conflict of interest.

Acknowledgements

The authors extend their appreciation to the Deputyship for Research & Innovation, Ministry of Education in Saudi Arabia for funding this research work through the project number: IF_2020_NBU_224.

References

1 Y. Hao, G. Sun, T. Fan, X. Tang, J. Zhang, Y. Liu, N. Zhang, L. Zhao, R. Zhong and Y. Peng, *J. Hazard. Mater.*, 2020, **399**, 122981.
2 Y. Xia, G. Wang, L. Guo, Q. Dai and X. Ma, *Chemosphere*, 2020, **241**, 125010.
3 M. Liang, R. Su, R. Huang, W. Qi, Y. Yu, L. Wang and Z. He, *ACS Appl. Mater. Interfaces*, 2014, **6**, 4638–4649.
4 Z. Farooqi, S. Khan and R. Begum, *Mater. Sci. Technol.*, 2017, **33**, 129–137.
5 K. Naseem, Z. H. Farooqi, R. Begum, M. Z. Ur Rehman, M. Ghufran, W. Wu, J. Najeeb and A. Irfan, *Environ. Sci. Pollut. Res.*, 2020, **27**, 28169–28182.
6 D. Zhang, H. Li, J. Li, Z. Xu, H. Liu, Y. Zhao, X. Feng and L. Chen, *Appl. Surf. Sci.*, 2020, **512**, 145668.
7 F. A. Plamper and W. Richtering, *Acc. Chem. Res.*, 2017, **50**, 131–140.
8 M. Shahid, Z. H. Farooqi, R. Begum, M. Arif, A. Irfan and M. Azam, *Chem. Phys. Lett.*, 2020, **754**, 137645.
9 M. Ajmal, S. Demirci, M. Siddiq, N. Aktas and N. Sahiner, *New J. Chem.*, 2016, **40**, 1485–1496.
10 H. Jia, D. Schmitz, A. Ott, A. Pich and Y. Lu, *J. Mater. Chem. A*, 2015, **3**, 6187–6195.
11 P. Ilgin, O. Ozay and H. Ozay, *Appl. Catal., B*, 2019, **241**, 415–423.
12 J.-F. Guillet, Z. Valdez-Nava, M. Golzio and E. Flahaut, *Carbon*, 2019, **146**, 542–548.
13 S. Owusu-Nkwantabisah, J. Gillmor, S. Switalski, M. R. Mis, G. Bennett, R. Moody, B. Antalek, R. Gutierrez and G. Slater, *Macromolecules*, 2017, **50**, 3671–3679.
14 Y. Wang, Z. Wang, K. Wu, J. Wu, G. Meng, Z. Liu and X. Guo, *Carbohydr. Polym.*, 2017, **168**, 112–120.
15 Y. Dong, Y. Ma, T. Zhai, F. Shen, Y. Zeng, H. Fu and J. Yao, *Macromol. Rapid Commun.*, 2007, **28**, 2339–2345.
16 S. Tang and J. Zheng, *Adv. Healthcare Mater.*, 2018, **7**, 1701503.
17 T. N. J. I. Edison, R. Atchudan, N. Karthik, J. Balaji, D. Xiong and Y. R. Lee, *Fuel*, 2020, **280**, 118682.
18 J. Ambreen, F. F. Al-Harbi, H. Sakhawat, M. Ajmal, H. Naeem, Z. H. Farooqi, N. Batool and M. Siddiq, *J. Mol. Liq.*, 2022, **355**, 118931.
19 A. Jouyban and E. Rahimpour, *Talanta*, 2020, **217**, 121071.

20 S. Davidović, V. Lazić, I. Vukoje, J. Papan, S. P. Anhrenkiel, S. Dimitrijević and J. M. Nedeljković, *Colloids Surf., B*, 2017, **160**, 184–191.
21 Z. H. Farooqi, S. R. Khan, T. Hussain, R. Begum, K. Ejaz, S. Majeed, M. Ajmal, F. Kanwal and M. Siddiq, *Korean J. Chem. Eng.*, 2014, **31**, 1674–1680.
22 M. Ajmal, Z. H. Farooqi and M. Siddiq, *Korean J. Chem. Eng.*, 2013, **30**, 2030–2036.
23 M. Ajmal, S. Anwar, H. Naeem, M. A. Zia and M. Siddiq, *Polym. Eng. Sci.*, 2020, **60**, 2918–2929.
24 T. Brändel, V. Sabadasch, Y. Hannappel and T. Hellweg, *ACS Omega*, 2019, **4**, 4636–4649.
25 L. Tzounis, M. Doña, J. M. Lopez-Romero, A. Fery and R. Contreras-Caceres, *ACS Appl. Mater. Interfaces*, 2019, **11**, 29360–29372.
26 S. Li, D. Lin, J. Zhou and L. Zha, *J. Phys. Chem. C*, 2016, **120**, 4902–4908.
27 S. Goggins, E. A. Apsey, M. F. Mahon and C. G. Frost, *Org. Biomol. Chem.*, 2017, **15**, 2459–2466.
28 A. Karimi, S. Husain, M. Hosseini, P. A. Azar and M. Ganjali, *Sens. Actuators, B*, 2018, **271**, 90–96.
29 K. B. Teodoro, F. L. Migliorini, W. A. Christinelli and D. S. Correa, *Carbohydr. Polym.*, 2019, **212**, 235–241.
30 R. G. Saratale, G. D. Saratale, S.-K. Cho, G. Ghodake, A. Kadam, S. Kumar, S. I. Mulla, D.-S. Kim, B.-H. Jeon and J. S. Chang, *J. Taiwan Inst. Chem. Eng.*, 2019, **99**, 239–249.
31 L. Qiu, F. Liu, L. Zhao, W. Yang and J. Yao, *Langmuir*, 2006, **22**, 4480–4482.
32 D.-M. Han, Q. M. Zhang and M. J. Serpe, *Nanoscale*, 2015, **7**, 2784–2789.
33 F. Bibi, M. Ajmal, F. Naseer, Z. Farooqi and M. Siddiq, *Int. J. Environ. Sci. Technol.*, 2018, **15**, 863–874.
34 J. Khan, M. Siddiq, B. Akram and M. A. Ashraf, *Arabian J. Chem.*, 2018, **11**, 897–909.
35 S. Sagbas and N. Sahiner, *Fuel Process. Technol.*, 2012, **104**, 31–36.
36 E. Costa, M. M. Lloyd, C. Chopko, A. Aguiar-Ricardo and P. T. Hammond, *Langmuir*, 2012, **28**, 10082–10090.
37 J. Brijitta, B. Tata and R. Joshi, *J. Polym. Res.*, 2015, **22**, 36.
38 M. Shibayama, Y. Fujikawa and S. Nomura, *Macromolecules*, 1996, **29**, 6535–6540.
39 Z. H. Farooqi, R. Begum, K. Naseem, U. Rubab, M. Usman, A. Khan and A. Ijaz, *Russ. J. Phys. Chem. A*, 2016, **90**, 2600–2608.
40 L. A. Shah, J. Ambreen, I. Bibi, M. Sayed and M. Siddiq, *J. Chem. Soc. Pak.*, 2016, **38**, 850–858.
41 S. R. Saeed, M. Ajmal, I. Bibi, S. S. Shah and M. Siddiq, *J. Taibah Univ. Sci.*, 2022, **16**, 472–479.
42 M. Ajmal, M. Siddiq, H. Al-Lohedan and N. Sahiner, *RSC Adv.*, 2014, **4**, 59562–59570.
43 R. Begum, Z. H. Farooqi, E. Ahmed, K. Naseem, S. Ashraf, A. Sharif and R. Rehan, *Appl. Organomet. Chem.*, 2017, **31**, e3563.
44 S. Jana, S. K. Ghosh, S. Nath, S. Pande, S. Praharaj, S. Panigrahi, S. Basu, T. Endo and T. Pal, *Appl. Catal., A*, 2006, **313**, 41–48.
45 M. I. Din, R. Khalid, Z. Hussain, T. Hussain, A. Mujahid, J. Najeeb and F. Izhar, *Crit. Rev. Anal. Chem.*, 2019, 1–17.
46 Z. H. Farooqi, K. Naseem, R. Begum and A. Ijaz, *J. Inorg. Organomet. Polym. Mater.*, 2015, **25**, 1554–1568.
47 Y. Li, J. Zhang, X. Ni, L. Wang and C. Yang, *Colloids Surf., A*, 2018, **538**, 818–824.
48 A. M. Atta, A. K. Gafer, H. A. Al-Lohedan, M. M. Abdullah and A. O. Ezzat, *Polym. Int.*, 2019, **68**, 1164–1177.
49 N. Cheng, Q. Hu, Y. Guo, Y. Wang and L. Yu, *ACS Appl. Mater. Interfaces*, 2015, **7**, 10258–10265.
50 A. Arshad, J. Iqbal, M. Siddiq, Q. Mansoor, M. Ismail, F. Mehmood, M. Ajmal and Z. Abid, *J. Appl. Phys.*, 2017, **121**, 024901.
51 W. Gong, Q. Wu, G. Jiang and G. Li, *J. Mater. Chem. A*, 2019, **7**, 13449–13454.
52 J. Feng, D. Fan, Q. Wang, L. Ma, W. Wei, J. Xie and J. Zhu, *Colloids Surf., A*, 2017, **520**, 743–756.
53 M. Beiranvand, S. Farhadi and A. Mohammadi, *Int. J. Nano Dimens.*, 2019, **10**, 180–194.
54 R. Rajamanikandan, K. Shanmugaraj and M. Ilanchelian, *J. Cluster Sci.*, 2017, **28**, 1009–1023.
55 M. M. Khan, J. Lee and M. H. Cho, *J. Ind. Eng. Chem.*, 2014, **20**, 1584–1590.
56 R. Vijayan, S. Joseph and B. Mathew, *IET Nanobiotechnol.*, 2018, **12**, 850–856.